

Imperfect detectors for adversarial tasks with applications to quantum key distribution

Shlok Nahar and Norbert Lütkenhaus

*Institute for Quantum Computing and Department of Physics and Astronomy,
University of Waterloo, Waterloo, Ontario, Canada, N2L 3G1*

(Dated: March 11, 2025)

Security analyses in quantum key distribution (QKD) and other adversarial quantum tasks often assume perfect device models. However, real-world implementations often deviate from these models. Thus, it is important to develop security proofs that account for such deviations from ideality. In this work, we develop a general framework for analysing imperfect threshold detectors, treating uncharacterised device parameters such as dark counts and detection efficiencies as adversarially controlled within some ranges. This approach enables a rigorous worst-case analysis, ensuring security proofs remain valid under realistic conditions. Our results strengthen the connection between theoretical security and practical implementations by introducing a flexible framework for integrating detector imperfections into adversarial quantum protocols.

I. INTRODUCTION

Many analyses of quantum information (QI) processing tasks rely on exact models of the devices used, particularly in adversarial applications like quantum key distribution (QKD). However, as we near the practical implementation of QI protocols, it is of increasing importance to perform more refined analyses that take into account experimental imperfections. In particular, devices cannot be perfectly characterised, and thus the theoretical analysis must account for cases involving only partial models. Moreover, for adversarial tasks such as QKD [1], entanglement verification [2], and quantum-secure multiparty deep learning [3], the adversary might even have some limited control over the devices. This further exacerbates the need for more refined theoretical analyses in the adversarial setting.

This has led to a growing attention to addressing imperfections in quantum devices, particularly in the context of QKD; both for realistic sources [4–8], and for realistic detection setups [9, 10]. While this body of work constitutes a tremendous amount of progress towards implementation security of QKD protocols, it is primarily restricted to the entropic uncertainty relation (EUR)- and phase-error correction-based proofs. On the other hand, work [5, 11] addressing imperfections compatible with entropy accumulation theorem-based proofs either assume qubit sources [11], or require bounds on quantities that cannot be easily related to physical device parameters [5]. Thus, it is important to develop methods that are more broadly applicable; both across proof techniques within QKD as well as for applications outside QKD.

In this work we address the problem of imperfect detection setups with threshold detectors in a general framework, leaving the problem of imperfect sources for future work. Our framework, introduced in Section III, treats imperfectly characterised device parameters equivalently to untrusted device parameters by ‘giving’ the uncharacterised component to Eve. This allows us to consider a ‘worst-case’ scenario with exact device parameters that can then use existing theoretical analyses. We emphasise that formally accomplishing this task is non-trivial as noticed in [12, Section V.B.] for the case of dark counts, and thus a rigorous analysis is needed. Furthermore, our framework relies solely on the intrinsic properties of the detection setup, without making any assumptions about the specific protocol in which the detection setup might be employed. Thus, we expect this to apply to adversarial tasks, in general.

We describe the techniques that allow for such a rigorous analysis for the case of dark counts and detector loss in Sections IV B 1 and IV B 2 respectively. Importantly, our results are presented in terms of experimentally measurable parameters, including the maximum dark count rate and the range of potential detector loss values. We also extend our analysis in Section IV B 3 to a form (Theorem 3) that can be applied for arbitrary imperfections, though the application of this generic result to practical situations is not immediately clear. Finally, we detail the application of our results to the various proof techniques for QKD in Section V.

II. DETECTOR MODEL

In this section, we describe a commonly used model for threshold detectors, and setups that utilise these detectors. Threshold detectors are devices that ideally ‘click’ in the presence of incident photons, and don’t click in the absence of incident photons. Deviations from ideality are termed dark counts, or detector efficiency as elaborated on in the following subsections.

A. Dark counts as classical post-processing

Dark counts are clicks that are registered by the detector in the absence of any incident photons. There are, broadly speaking, two mechanisms that explain this phenomenon. Firstly, single-photon detectors sometimes have dark counts as a result of thermal noise, where thermally generated carriers or quantum tunneling of electrons can cause spurious detections [13]. This results in dark counts that are independent of any other click events. Secondly, after a click event, SPAD detectors sometimes have trapped charges that are released at a later time causing additional click events, commonly called afterpulsing [14]. In this work, we deal with the effect of dark counts that are independent of other click events, and each other.

The independent dark counts can be modelled as a classical post-processing being applied to the measurement outcomes. For example, consider a single threshold detector with dark count rate d_B having POVM $\{\Gamma_{\text{nc}}^{d_B}, \Gamma_{\text{c}}^{d_B}\}$ corresponding to click and no-click events respectively. This can be written in terms of the POVM $\{\Gamma_{\text{nc}}, \Gamma_{\text{c}}\}$ of a threshold detector without dark counts as

$$\begin{aligned}\Gamma_{\text{nc}}^{d_B} &= (1 - d_B)\Gamma_{\text{nc}} \\ \Gamma_{\text{c}}^{d_B} &= \Gamma_{\text{c}} + d_B\Gamma_{\text{nc}}.\end{aligned}\tag{1}$$

Equation (1) can be more concisely written as

$$\vec{\Gamma}_{d_B} = \mathcal{P}^{d_B}\vec{\Gamma},\tag{2}$$

where $\mathcal{P}^{d_B} = \begin{pmatrix} 1 - d_B & 0 \\ d_B & 1 \end{pmatrix}$ is a stochastic matrix that describes the classical post-processing, and $\vec{\Gamma} = \begin{pmatrix} \Gamma_{\text{nc}} \\ \Gamma_{\text{c}} \end{pmatrix}$. Similarly, for a more general detection setup with k threshold detectors, we can write the post-processing map acting on all 2^k click patterns based on the dark count rates $\mathbf{d}_{\mathbf{B}} = (d_1, d_2, \dots, d_k)$ as $\mathcal{P}^{\mathbf{d}_{\mathbf{B}}}$. While the exact structure of $\mathcal{P}^{\mathbf{d}_{\mathbf{B}}}$ is not important, we shall comment on the relevant properties of $\mathcal{P}^{\mathbf{d}_{\mathbf{B}}}$ where applicable. In this work, we will refer to the (i, j) element of a post-processing matrix \mathcal{P} as $\mathcal{P}_{i|j}$ to represent the probability of outcome (alternately, click pattern) i given outcome (alternately, click pattern) j .

B. Modeling detector efficiency

Detector efficiency refers to the fact that the detector does not always register a click when photons are incident on it. In this work, we assume that the detector efficiency is independent of prior detection events. A typical quantum optical model for detection efficiency uses the single-photon detection efficiency η , which represents the probability of the detector registering a click for each incident photon. This can also be represented as a beam splitter with transmission amplitude coefficient $\sqrt{\eta}$, followed by a lossless detector.

An important special case that we shall use in this work, is that of a lossy detector, with no dark counts with an input with *no more than a single photon*. This case might sound oddly specific, but its usage will become clearer in Section IV B 2. In this case, the loss can be represented as a classical post-processing analogous to Eq. (2)

$$\vec{\Gamma}_{\eta} = \mathcal{P}^{\eta}\vec{\Gamma},\tag{3}$$

where $\mathcal{P}^{\eta} = \begin{pmatrix} 1 & 1 - \eta \\ 0 & \eta \end{pmatrix}$, and $\vec{\Gamma} = \begin{pmatrix} \Gamma_{\text{nc}} \\ \Gamma_{\text{c}} \end{pmatrix}$. Similarly, for a more general detection setup with k threshold detectors, we can write the post-processing map $\mathcal{P}^{\boldsymbol{\eta}}$ acting on all 2^k click patterns based on the loss of each detector $\boldsymbol{\eta} = (\eta_1, \eta_2, \dots, \eta_k)$. Note once again that this post-processing map is valid for detectors without dark counts, with an input with no more than a single photon.

III. SQUASHING MAPS AND NOISE CHANNELS

We first give a brief, intuitive overview of the core idea of our framework, which is inspired by squashing maps [15–18], before explaining the details. For an arbitrary detection setup with dark count rates $\mathbf{d}_{\mathbf{B}}$ and loss $\boldsymbol{\eta}$, we wish to construct a “noise channel” $\Phi_{\mathbf{d}_{\mathbf{B}}, \boldsymbol{\eta}}$ such that $\text{Tr}[\vec{\Gamma}_{\mathbf{d}_{\mathbf{B}}, \boldsymbol{\eta}}\rho] = \text{Tr}[\vec{\Gamma}\Phi_{\mathbf{d}_{\mathbf{B}}, \boldsymbol{\eta}}(\rho)]$ for all input quantum states ρ . Informally, we wish to model the noisy detection setup as a noise channel followed by an ideal detection setup.

The existence of such a channel is often sufficient to simplify the analysis for applications such as entanglement verification [19] and QKD. Intuitively, this is because the noise channel can be ‘given’ to the adversary. For example,

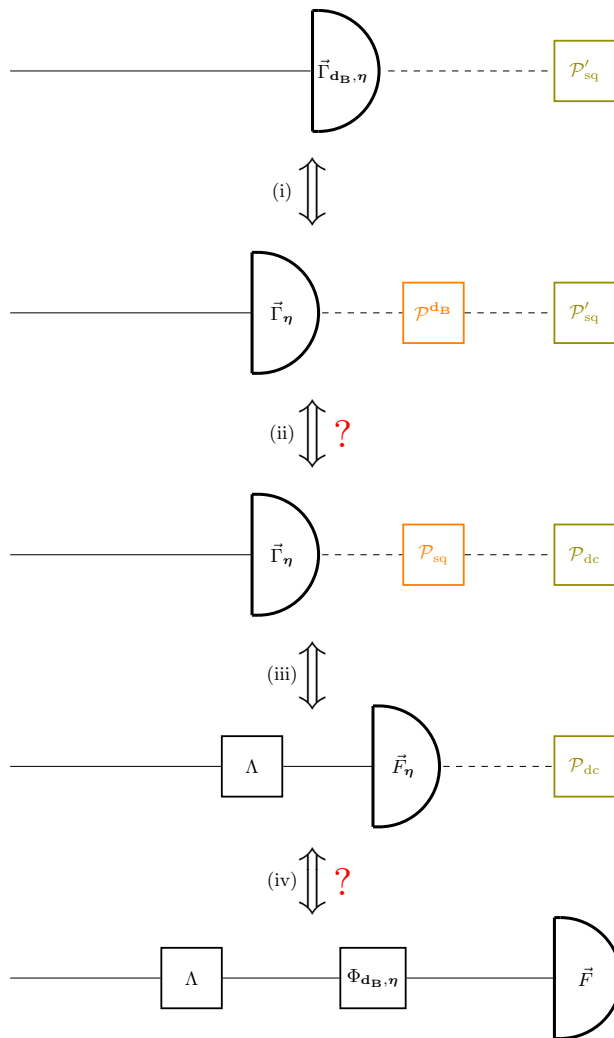


FIG. 1. A set of equivalences (as quantum-to-classical measurement channels) of detection setups to consider dark counts as part of the noise channel. Here, \mathcal{P}'_{sq} represents the classical post-processing carried out in the protocol, \mathcal{P}^{dB} is the dark count post-processing, \mathcal{P}_{sq} is the post-processing required for the existence of the squashing map Λ , and \mathcal{P}_{dc} is the post-processing fixed by Eq. (4). In the figure, olive post-processing maps represent free choices that can be made to make equivalences (ii) and (iv) hold. Orange post-processing maps represent stochastic processes fixed by equivalences (i) and (iii).

in QKD the security of a protocol using noisy POVM $\vec{\Gamma}_{dB,\eta}$ would directly follow from the security of a protocol using ideal POVM \vec{F} along with the existence of a noise channel (See Lemma 6 from Ref. [20] for a proof).

However, we were unable to generically construct a noise channel acting on the full Fock space. Thus, to simplify our task we make use of squashing maps [18, 21]. The general framework that we employ is shown in Figure 1. Each equivalence is an equivalence of quantum-to-classical measurement channels.

- We start by considering a generic detection setup that uses threshold detectors with dark counts and loss. Additionally, we allow for some classical post-processing \mathcal{P}'_{sq} . We elaborate more on this choice later.
- Equivalence (i) follows from the fact that dark counts can be modelled as a classical post-processing \mathcal{P}^{dB} as described in Section II A.
- Part of our task is to show that equivalence (ii) holds for some choice of \mathcal{P}_{dc} and a fixed \mathcal{P}_{sq} , as discussed in detail in Section III 1.
- Equivalence (iii) assumes that there exists a squashing model [18, 21] for the particular detection setup being considered together with the specific \mathcal{P}_{sq} fixed through equivalence (ii). Although, the simple squashers described in Ref. [18] have been shown to exist only under some restrictions on the detection setup, the flag-state squasher

[21] and the weight-preserving flag-state squasher (WPFSS) [20, Lemma 7] always exist for detection setups using threshold detectors.

- It is then left to show that equivalence (iv) holds, which is discussed in detail in Section III 2.

1. *Does equivalence (ii) hold?*

\mathcal{P}_{sq} is the post-processing required for the specific squashing map we wish to use. For example, for an active BB84 detection setup, we can use Theorem 10 from Ref. [18] to obtain the post-processing $\mathcal{P}_{\text{sq}} = \begin{pmatrix} 1 & 0 & 0 & 0 \\ 0 & 1 & 0 & 1/2 \\ 0 & 0 & 1 & 1/2 \end{pmatrix}$ which maps double clicks in a particular basis to random single clicks in the same basis. $\mathcal{P}^{\mathbf{dB}}$ is the dark count post-processing for the detection setup. Thus, the equivalence amounts to asking if there exist stochastic matrices $\mathcal{P}'_{\text{sq}}, \mathcal{P}_{\text{dc}}$ such that

$$\mathcal{P}'_{\text{sq}} \mathcal{P}^{\mathbf{dB}} = \mathcal{P}_{\text{dc}} \mathcal{P}_{\text{sq}}. \quad (4)$$

Note that \mathcal{P}'_{sq} can be freely chosen by physically performing the appropriate classical post-processing on the measurement results. For simplicity, we choose $\mathcal{P}'_{\text{sq}} = \mathcal{P}_{\text{sq}}$ in this work. We shall comment more on the post-processing \mathcal{P}_{sq} needed for the flag-state squasher and the WPFSS in Section V A.

2. *Does equivalence (iv) hold?*

This equivalence can be formally stated as

$$\mathcal{P}_{\text{dc}} \text{Tr}[\vec{F}_{\boldsymbol{\eta}} \rho] = \text{Tr}[\vec{F} \Phi_{\mathbf{dB}, \boldsymbol{\eta}}(\rho)], \quad (5)$$

for all density matrices ρ in the squashed space. Here, $\vec{F}_{\boldsymbol{\eta}}$ is the squashed lossy POVM which satisfies $\Lambda^\dagger(\vec{F}_{\boldsymbol{\eta}}) = \vec{\Gamma}_{\boldsymbol{\eta}}$, and \vec{F} is the ideal target POVM.

Thus, we have a framework that allows us to reduce the analysis of a detection setup with dark counts and loss $\vec{\Gamma}_{\mathbf{dB}, \boldsymbol{\eta}}$ to that of a squashed ideal POVM \vec{F} . This reduction follows simply by checking if Eqs. (4) and (5) hold. For completeness, in Appendix A we give a general method to numerically check if Eqs. (4) and (5) hold, given a specific value of \mathbf{dB} and $\boldsymbol{\eta}$.

A. Pedagogical example - Active BB84 detection setup with lossless detectors

We illustrate the use of our framework via the concrete example of the active BB84 detection setup, using the simple squasher described in [18, Theorem 10]. For the purpose of this example, we assume lossless detectors.

We first analyse equivalence (ii) for each basis choice separately. The dark count post-processing for this setup is

$$\mathcal{P}^{\mathbf{dB}} = \begin{pmatrix} (1-d_1)(1-d_2) & 0 & 0 & 0 \\ d_1(1-d_2) & (1-d_2) & 0 & 0 \\ d_2(1-d_1) & 0 & (1-d_1) & 0 \\ d_1 d_2 & d_2 & d_1 & 1 \end{pmatrix}. \text{ Also, recall that the squashing post-processing for this protocol is}$$

$$\mathcal{P}_{\text{sq}} = \begin{pmatrix} 1 & 0 & 0 & 0 \\ 0 & 1 & 0 & 1/2 \\ 0 & 0 & 1 & 1/2 \end{pmatrix}.$$

We make the simplifying choice $\mathcal{P}'_{\text{sq}} = \mathcal{P}_{\text{sq}}$, and compute

$$\mathcal{P}_{\text{sq}} \mathcal{P}^{\mathbf{dB}} = \begin{pmatrix} (1-d_1)(1-d_2) & 0 & 0 & 0 \\ d_1(1-d_2/2) & 1-d_2/2 & d_1/2 & 1/2 \\ d_2(1-d_1/2) & d_2/2 & 1-d_1/2 & 1/2 \end{pmatrix}. \quad (6)$$

We then attempt to construct \mathcal{P}_{dc} so that it satisfies Eq. (4). First, we can write $\mathcal{P}_{\text{sq}} = (\mathbb{I}_3 \ v)$, where $v = \begin{pmatrix} 0 \\ 1/2 \\ 1/2 \end{pmatrix}$. Then,

$$\mathcal{P}_{\text{dc}}\mathcal{P}_{\text{sq}} = (\mathcal{P}_{\text{dc}} \ u), \quad (7)$$

where $u = \mathcal{P}_{\text{dc}}v$. As can be seen from Eqs. (6) and (7), Eq. (4) can only hold if

$$\mathcal{P}_{\text{dc}} = \begin{pmatrix} (1-d_1)(1-d_2) & 0 & 0 \\ d_1(1-d_2/2) & 1-d_2/2 & d_1/2 \\ d_2(1-d_1/2) & d_2/2 & 1-d_1/2 \end{pmatrix}, \quad (8)$$

which in turn implies that

$$u = \begin{pmatrix} 0 \\ 1/2 + \frac{d_1-d_2}{2} \\ 1/2 + \frac{d_2-d_1}{2} \end{pmatrix}. \quad (9)$$

Note that this does *not* satisfy Eq. (4) unless $d_1 = d_2 =: d$. Thus, we must assume that the dark count rates of both detectors are exactly the same to use this framework with the qubit squasher.

Although this assumption is not met in practice, we nonetheless elaborate on this example due to its pedagogical value in illustrating our general framework. In Section IV we shall avoid this assumption by using the flag-state squasher instead.

Moving our attention to the construction of the noise channel described in equivalence (iv), we construct the map

$$\begin{aligned} \Phi_{\mathbf{dB}}(\rho) &= \text{Tr}[\rho |\text{vac}\rangle\langle\text{vac}|] \left((1-d)^2 |\text{vac}\rangle\langle\text{vac}| + d(1-d/2) \Pi \right) \\ &\quad + (1-d) \Pi \rho \Pi + \text{Tr}[\Pi \rho \Pi] d \frac{\Pi}{2}, \end{aligned} \quad (10)$$

where Π is the projection onto the qubit space. It can easily be verified that this guess is a valid channel by writing it as a QND measurement, followed by state preparation and depolarizing channels.

Finally, explicit computations give us that Eq. (5) is satisfied by this channel. We sketch the computations for a single basis here. First consider the POVM elements $F_{\text{nc}} = |\text{vac}\rangle\langle\text{vac}|$, $F_0 = |0\rangle\langle 0|$, and $F_1 = |1\rangle\langle 1|$. From Eq. (8), we obtain

$$\mathcal{P}_{\text{dc}} \text{Tr} \left[\vec{F} \rho \right] = \begin{pmatrix} (1-d)^2 \text{Tr}[\rho |\text{vac}\rangle\langle\text{vac}|] \\ d(1-d/2) \text{Tr}[\rho |\text{vac}\rangle\langle\text{vac}|] + (1-d/2) \text{Tr}[\rho |0\rangle\langle 0|] + d/2 \text{Tr}[\rho |1\rangle\langle 1|] \\ d(1-d/2) \text{Tr}[\rho |\text{vac}\rangle\langle\text{vac}|] + d/2 \text{Tr}[\rho |0\rangle\langle 0|] + (1-d/2) \text{Tr}[\rho |1\rangle\langle 1|] \end{pmatrix}. \quad (11)$$

The claim $\text{Tr} \left[\vec{F} \Phi_{\mathbf{dB}}(\rho) \right] = \mathcal{P}_{\text{dc}} \text{Tr} \left[\vec{F} \rho \right]$ then follows from Eqs. (10) and (11) by noting that $\Pi |0\rangle = |0\rangle$ and $\Pi |1\rangle = |1\rangle$. A similar computation for the $+/-$ basis gives us that Eq. (5) is satisfied for this noise channel.

Thus, we have shown by explicit construction, the existence of a noise channel for the active BB84 setup using a simple squasher [18, Theorem 10], under the assumption that both the lossless detectors have the same dark count rate. We will now extend this analysis to the more practical scenario where the loss and dark count rates of detectors may differ from each other by using the flag-state squasher.

IV. NOISE CHANNEL WITH FLAG-STATE SQUASHER

In this section, we introduce the flag-state squasher [21] in Section IV A to generalise the pedagogical example described in Section III A to the scenario with unequal loss and dark count rates (Sections IV B 1 and IV B 2). Furthermore, we extend our analysis to more generic setups in Section IV B 3.

A. Flag-state squasher

The flag-state squasher [21, Theorem 1] is a squashing map (equivalence (iii) in Fig. 1) that generalises the simple squasher [16, 18] for arbitrary detection setups where the POVM elements have a block-diagonal structure. For

detection setups using threshold detectors, such a block-diagonal structure arises naturally where the blocks correspond to total photon number:

$$\Gamma_i = \Gamma_{i,0} \oplus \Gamma_{i,0 < m \leq N} \oplus \Gamma_{i,m > N}.$$

Here, $m > N$ corresponds to the set of photon-numbers m greater than the cutoff N , and $\Gamma_{i,0}$ acts on the space spanned by the vacuum state $|\text{vac}\rangle$. Although separating out the vacuum space does not affect the squashing — the space spanned by the states with photon number $m \leq N$ can correspond to a single block — we explicitly separate the vacuum space as it simplifies the notation later. The target measurements are given by

$$F_i = \Gamma_{i,0} \oplus \Gamma_{i,0 < m \leq N} \oplus |i\rangle\langle i|,$$

where $\{|i\rangle\}_{i=0}^{n_{\text{meas}}-1}$ forms an orthonormal set of vectors termed ‘flags’. We denote the space spanned by $\{\Gamma_{i,0 < m \leq N}\}_{i=1}^{n_{\text{meas}}}$ as $\mathcal{H}_{0 < m \leq N}$, the space spanned by the vacuum state as \mathcal{H}_0 , and the space spanned by the flags as \mathcal{H}_F . We call $\mathcal{H}_0 \oplus \mathcal{H}_{0 < m \leq N}$ the preserved subspace, and \mathcal{H}_F the flag space.

Note that in adversarial applications, the idea is to ‘give’ the eavesdropper Eve the squashing map so that the analysis can then be restricted to the finite-dimensional POVM elements. However, in the case of the flag-state squasher the existence of the flags implies that there exists a classical state [22] living entirely in the flag subspace that results in a given probability distribution when measured, for all probability distributions. Thus, giving Eve full control over the flag-state squasher would result in a complete loss of any ‘quantumness’ of the quantum information protocol (since any observations can be completely explained by classical states). A common solution is to add an additional constraint that bounds the weight W in the flag space, intuitively bounding the extent to which a classical flag state can explain observations.

The canonical method of bounding the weight outside the preserved subspace can be found in Ref. [23] and proceeds as follows. For any event e , and any input state ρ it can be shown that

$$W \leq 1 - \text{Tr}[\rho \Pi_N] \leq \frac{p(e) - \lambda_{\min}(\Pi_N \Gamma_e \Pi_N)}{\lambda_{\min}(\overline{\Pi}_N \Gamma_e \overline{\Pi}_N) - \lambda_{\min}(\Pi_N \Gamma_e \Pi_N)}, \quad (12)$$

where Π_N ($\overline{\Pi}_N$) is the projection on (outside) the space corresponding to $\Gamma_{i,m \leq N}$. Note that the choice of this event e need not be a single POVM element (alternately, click-pattern), it could also be some ‘coarse-graining’ that includes multiple click-patterns. Thus, there is a large amount of freedom when choosing this event.

When working with the infinite-dimensional POVM, some protocol-dependent choices [12, 24] for the event e lead to good bounds on the weight W . This bound can then be added in as an additional constraint to the finite-dimensional analysis. More recently, Ref. [25, Section VII. F.] shows that this event e can be chosen to be the multi-click event, i.e. all click patterns that consist of more than a single click in the various detectors, for arbitrary passive optical setups. This is the choice we shall focus on in Section V A due to its generality.

Thus, our task can be broken up into two parts as shown in Fig. 2. First, we need to show that there exists a noise channel $\Phi_{\mathbf{dB},\eta}$ such that Eq. (5) is satisfied. Next, we need to find the weight outside the preserved space $W^{\mathbf{dB},\eta}$ after the application of the noise channel. In other words, given that $W \leq 1 - \text{Tr}[\rho \Pi_N]$ for any input state ρ , we need to find $W^{\mathbf{dB},\eta} \leq 1 - \text{Tr}[\Phi_{\mathbf{dB},\eta}(\rho) \Pi_N]$.

Note that unlike the qubit squasher, the flag-state squasher does not depend on some post-processing \mathcal{P}_{sq} for its existence. Thus, Fig. 2 does not contain equivalence (ii) from Fig. 1. However, we might sometimes wish to ‘coarse-grain’ the data before using the flag-state squasher. In this case, we would need to also prove equivalence (ii) (from Fig. 1) for the coarse-graining post-processing. However, for the sake of pedagogy, we will first perform our analysis without any such complications before discussing the impact of coarse-graining in Section V A.

B. Construction of Noise Channel

We shall construct the full noise channel $\Phi_{\mathbf{dB},\eta}$ in two steps. First we construct a noise channel for the dark counts $\Phi_{\mathbf{dB}}$, and then another for the loss Φ_{η} .

1. Noise channel for dark counts

Any detection setup has single-click events, defined as events where only a single detector clicks, and multi-click events, defined as events where more than one detector clicks. We let S be the set of single-click events, and M be

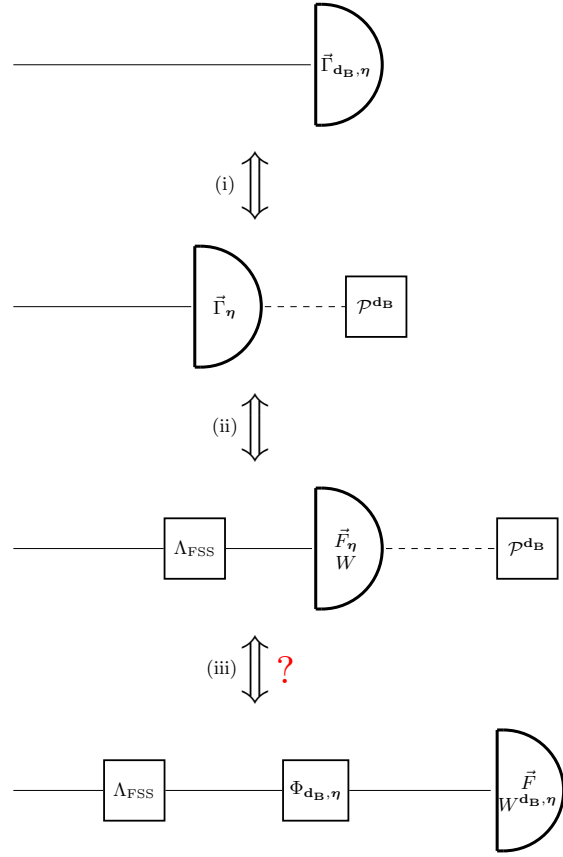


FIG. 2. A set of equivalences (as quantum-to-classical measurement channels) of detection setups to consider dark counts as part of the noise channel, using the flag-state squasher.

the set of multi-click events. The no-click event will always be denoted by the event 0. The set of all events will be denoted by U .

We first list a set of sufficient conditions we require from the classical post-processing \mathcal{P}^{dB} in order to construct the noise channel. We then physically motivate these conditions.

1. The post-processing does not turn one single-click event into another, i.e.,

$$\mathcal{P}_{s|s'}^{\text{dB}} = 0, \quad (13)$$

for all distinct $s, s' \in S$.

2. The post-processing does not turn any click event into a no-click event, i.e.,

$$\mathcal{P}_{0|i}^{\text{dB}} = 0, \quad (14)$$

for all $i \neq 0$.

3. The post-processing is such that

$$\mathcal{P}_{s|s}^{\text{dB}} \geq \mathcal{P}_{0|0}^{\text{dB}}, \quad (15)$$

for all $s \in S$.

The first two conditions are true for any dark count post-processing as dark counts do not stop a detector from clicking. To see why the third condition is true, observe that $\mathcal{P}_{s|s}^{\text{dB}} = \prod_{i \neq s} (1 - d_i)$ is the probability that none of the other detectors have a dark count. On the other hand, $\mathcal{P}_{0|0}^{\text{dB}} = \prod_i (1 - d_i)$ is the probability that none of the detectors have a dark count. Since $(1 - d_s) \leq 1$, the claim follows.

We also need to make an additional assumption on the POVM without dark counts $\vec{\Gamma}_\eta$. Informally, the assumption is that we cannot have more clicks than photons. More formally, this can be expressed as

$$\begin{aligned}\mathrm{Tr}[\Gamma_m^\eta \rho_1] &= 0 \\ \mathrm{Tr}[\Gamma_m^\eta |\mathrm{vac}\rangle\langle\mathrm{vac}|] &= 0 \\ \mathrm{Tr}[\Gamma_s^\eta |\mathrm{vac}\rangle\langle\mathrm{vac}|] &= 0,\end{aligned}\tag{16}$$

for all $m \in M$, $s \in S$ and any single-photon state ρ_1 . This naturally holds for typical detection setups as dark counts are the only way single photons can result in multiple detectors clicking or vacuum can result in any detector clicking. Note that this immediately implies that $\mathrm{Tr}[\Gamma_0 |\mathrm{vac}\rangle\langle\mathrm{vac}|] = 1$.

We combine all these properties to define a generic optical detection setup.

Definition 1 (Threshold detection setup with independent dark counts). We define the POVM $\vec{\Gamma}_{\mathbf{d}_B, \eta}$ to be a *threshold detection setup with independent dark counts* if

1. it is equivalent to a a POVM without dark counts $\vec{\Gamma}_\eta$ followed by a dark count post-processing $\mathcal{P}^{\mathbf{d}_B}$ as described in equivalence (i) of Fig. 2,
2. the dark count post-processing satisfies Eqs. (13) to (15), and
3. the POVM without dark counts $\vec{\Gamma}_\eta$ satisfies Eq. (16).

We now have all the tools to construct the noise channel for dark counts.

Theorem 1 (Dark count noise channel). Let $\vec{\Gamma}_{\mathbf{d}_B, \eta}$ be the POVM for a threshold detection setup with independent dark counts, where each $\Gamma_i^{\mathbf{d}_B, \eta} = \Gamma_{i,0}^{\mathbf{d}_B, \eta} \oplus \Gamma_{i,m=1}^{\mathbf{d}_B, \eta} \oplus \Gamma_{i,m>1}^{\mathbf{d}_B, \eta}$ is block-diagonal with an associated Hilbert space $\mathcal{H}_0 \oplus \mathcal{H}_1 \oplus \mathcal{H}_{m>1}$ corresponding to the total photon number. Then there exists a flag-state squashing map $\Lambda : \mathcal{H}_0 \oplus \mathcal{H}_1 \oplus \mathcal{H}_{m>1} \rightarrow \mathcal{H}_{m \leq 1} \oplus \mathcal{H}_F$, and a noise channel $\Phi_{\mathbf{d}_B} : \mathcal{H}_0 \oplus \mathcal{H}_1 \oplus \mathcal{H}_F \rightarrow \mathcal{H}_0 \oplus \mathcal{H}_1 \oplus \mathcal{H}_F$ such that $\mathrm{Tr}[\vec{\Gamma}_{\mathbf{d}_B, \eta} \rho] = \mathrm{Tr}[\vec{F}_\eta \Phi_{\mathbf{d}_B}(\Lambda(\rho))]$ for all density matrices ρ . Here,

$$F_i^\eta = \Gamma_{i,m=0}^\eta \oplus \Gamma_{i,m=1}^\eta \oplus |i\rangle\langle i|,$$

where $|i\rangle$ forms an orthonormal basis for the flag space \mathcal{H}_F . Moreover for any density matrix ρ ,

$$\mathrm{Tr}[\Phi_{\mathbf{d}_B}(\rho) \Pi_{\leq 1}] = \mathcal{P}_{0|0}^{\mathbf{d}_B} \mathrm{Tr}[\rho \Pi_{\leq 1}],\tag{17}$$

where $\Pi_{\leq 1}$ is the projection onto the space $\mathcal{H}_0 \oplus \mathcal{H}_1$, and $\mathcal{P}^{\mathbf{d}_B}$ is the stochastic matrix that models the dark counts.

The proof is given in Appendix B.

Recall that equivalence (iii) in Fig. 2 required the existence of a noise channel $\Phi_{\mathbf{d}_B, \eta}$, and a bound on the weight outside the preserved subspace $W^{\mathbf{d}_B, \eta}$ after the application of the noise channel. Theorem 1 is the first step towards equivalence (iii), showing that there exists a noise channel $\Phi_{\mathbf{d}_B}$ for dark counts, and relating the weight outside the preserved subspace before and after the application of the dark count noise channel through Eq. (17) — $W^{\mathbf{d}_B} = 1 - \mathcal{P}_{0|0}^{\mathbf{d}_B}(1 - W)$. We now prove an analogous result for lossy detectors.

2. Noise channel for loss

Theorem 2 (Loss noise channel). Let $\vec{\Gamma}_\eta$ be the POVM for a threshold detection setup with loss (and without dark counts), where for each POVM outcome i , $\Gamma_i^\eta = \Gamma_{i,m \leq 1}^\eta \oplus \Gamma_{i,m > 1}^\eta$ is block-diagonal with an associated Hilbert space $\mathcal{H}_{m \leq 1} \oplus \mathcal{H}_{m > 1}$ corresponding to the total photon number. Let η_{\min} and η_{\max} be the minimum and maximum of all the detector efficiencies used in the detection setup. We can then define a family of noise channels $\Phi_\eta^{\eta^*}$ and target POVMs \vec{F}_{η^*} parametrised by some parameter η^* as follows. For any value of $\eta^* \in \left[\frac{\eta_{\min}}{1 - (\eta_{\max} - \eta_{\min})}, 1 \right]$, there exists a flag-state squashing map $\Lambda : \mathcal{H}_{m \leq 1} \oplus \mathcal{H}_{m > 1} \rightarrow \mathcal{H}_{m \leq 1} \oplus \mathcal{H}_F$, and a noise channel $\Phi_\eta^{\eta^*} : \mathcal{H}_{m \leq 1} \oplus \mathcal{H}_F \rightarrow \mathcal{H}_{m \leq 1} \oplus \mathcal{H}_F$ such that $\mathrm{Tr}[\vec{\Gamma}_\eta \rho] = \mathrm{Tr}[\vec{F}_{\eta^*} \Phi_\eta^{\eta^*}(\Lambda(\rho))]$ for all density matrices ρ . Here,

$$F_i^{\eta^*} = \Gamma_{i,m \leq 1}^{\eta^*} \oplus |i\rangle\langle i|,$$

where $|i\rangle$ forms an orthonormal basis for the flag space \mathcal{H}_F , and $\vec{\Gamma}_{\eta^*}$ is the POVM with (common) efficiency η^* in all detectors. Moreover for any density matrix ρ ,

$$\text{Tr}\left[\Phi_{\eta^*}^{\eta^*}(\rho)\Pi_{\leq 1}\right] = \frac{\eta_{\min}}{\eta^*} \text{Tr}[\rho\Pi_{\leq 1}], \quad (18)$$

where $\Pi_{\leq 1}$ is the projection onto the space $\mathcal{H}_{m\leq 1}$.

The proof is given in Appendix B.

Note that Theorem 2 leaves us with some freedom to choose how we define the ‘ideal’ POVM \vec{F}_{η^*} . Increasing the efficiency η^* of the ideal POVM decreases the weight $\frac{\eta_{\min}}{\eta^*}$ of the state in the preserved subspace. Additional work must be done to decide what the optimal choice would be. Intuitively, we would expect that the optimal choice would maximise the weight in the preserved subspace, as any part of the state outside the preserved subspace is entirely classical. For notational simplicity, we refer to the noise channel $\Phi_{\eta^*}^{\eta^*}$ simply as Φ_{η} .

Finally, combining Theorems 1 and 2 gives us the noise channel $\Phi_{\mathbf{d}_B, \eta} = \Phi_{\eta} \circ \Phi_{\mathbf{d}_B}$ required for equivalence (iii). The above theorems additionally relate the weight outside the preserved subspace before and after the application of the dark count noise channel through Eqs. (17) and (18) — $W^{\mathbf{d}_B, \eta} = 1 - \mathcal{P}_{0|0}^{\mathbf{d}_B} \frac{\eta_{\min}}{\eta^*} (1 - W)$.

Note that the usage of this theorem towards equivalence (iii) still requires a bound on the weight outside the preserved subspace W before the application of the noise channel. Although this bound can be obtained independent of the dark count rates \mathbf{d}_B as shown in [12, Appendix A] and [25, Corollary 4], an analogous (setup-independent) result independent of detector loss does not yet exist. Thus, this would need to be analysed individually for different detection setups, for instance by minimising the bounds obtained from [25, Theorem 3] over all allowed values of loss.

3. Noise channel for generic setup imperfections

We will now state a theorem that can account for more generic detection setup imperfections, inspired by the proof of Theorem 1. At an intuitive level, the proof first decomposes the noisy POVM into an ideal POVM (with some probability p), and a non-ideal POVM (with probability $1 - p$). Then, we ‘turn’ the non-ideal POVM into a flag through the noise channel, and are only left analysing the ideal POVM. This intuitive idea is formalised in the following theorem.

Theorem 3 (Generic noise channel). Let the flag-state squashed POVM \vec{F}_{noise} describing the actual imperfect detection setup be related to an ideal flag-state squashed POVM \vec{F}_{ideal} as

$$\vec{F}_{\text{noise}} - (1 - q)\vec{F}_{\text{ideal}} \geq 0, \quad (19)$$

for some $q \in [0, 1]$. Then there exists a noise channel Φ_{noise} such that the following equations hold for any state ρ :

$$\text{Tr}\left[\vec{F}_{\text{noise}} \rho\right] = \text{Tr}\left[\vec{F}_{\text{ideal}} \Phi_{\text{noise}}(\rho)\right] \quad (20)$$

$$\text{Tr}[\Pi\rho] = (1 - q) \text{Tr}[\Pi\Phi_{\text{noise}}(\rho)], \quad (21)$$

where Π is the projection onto the preserved subspace.

Unlike the other theorems, we leave the proof of this theorem in the main text as we believe the proof is simple to understand and instructive.

Proof. First, note that Eq. (19) implies that there exists a POVM \vec{Q} such that

$$\vec{F}_{\text{noise}} = (1 - q)\vec{F}_{\text{ideal}} + q\vec{Q}.$$

We use this POVM to construct the noise channel as depicted in Fig. 3:

$$\Phi_{\text{noise}}\left(\left(\begin{array}{c|c} \rho_P & B \\ \hline B^\dagger & \rho_F \end{array}\right)\right) := (1 - q)\rho_P \oplus \left(q \sum_i \text{Tr}[\rho_P Q_i] |i\rangle\langle i| + \rho_F\right), \quad (22)$$

where $|i\rangle\langle i|$ are the flag states corresponding to measurement outcome i . It is straightforward to verify that Eqs. (20) and (21) hold for this noise channel. \square

Theorem 3 has a number of noteworthy features as listed below.

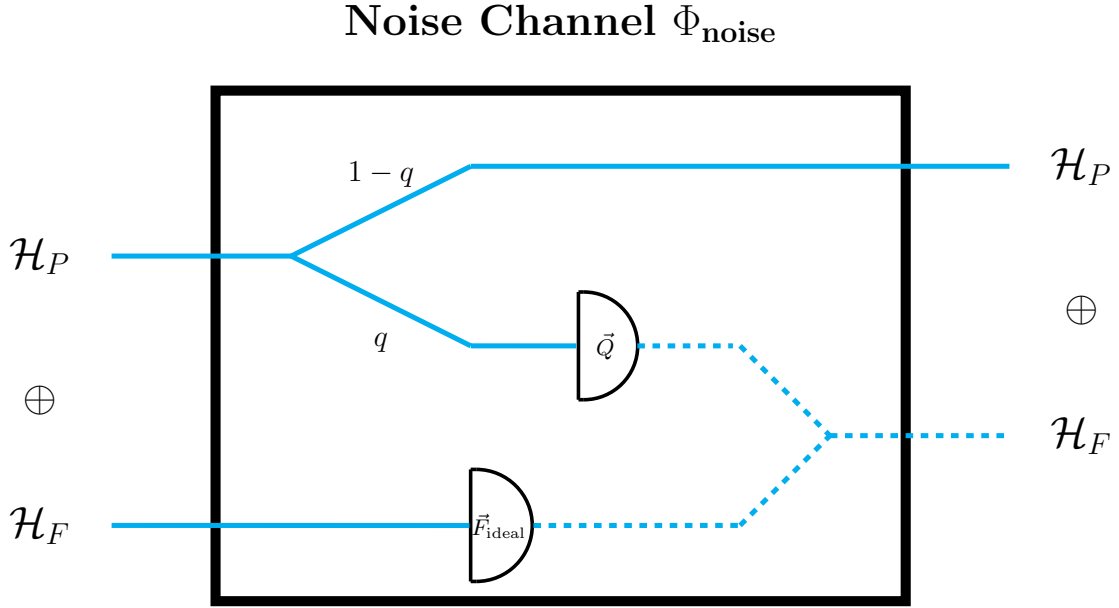


FIG. 3. Constructive description of the noise channel. Each line corresponds to a subspace of the input Hilbert space associated with the block-diagonal decomposition of the POVM elements. The dashed lines refer to classical states. \mathcal{H}_P and \mathcal{H}_F refer to the preserved and flag spaces respectively.

1. **Noisy POVM \vec{F}_{noise} :** We have generically termed this a noisy POVM. This could be noisy either due to imperfection characterisation, or due to Eve having some limited control over them. Both are treated equivalently in our framework.
2. **Ideal POVM \vec{F}_{ideal} :** There is a large amount of freedom in choosing this ‘ideal’ POVM. The choice of common efficiency η^* in Theorem 2 was a manifestation of this degree of freedom. There are two competing factors when making this choice of POVM. First the ideal POVM should be useful for the application being analysed. Second, the choice of ideal POVM would influence how ‘close’ the noisy POVM is to the ideal POVM, and thus the ‘cost’ of using Theorem 3 through Eq. (12) as expanded on in the next point.
3. **Deviation from ideality q :** Given a choice of ideal POVM \vec{F}_{ideal} , the optimal choice of q is simply the minimum value that still satisfies Eq. (19). This can be seen by noting that the weight in the flag space consists entirely of classical states. Thus, for most quantum information applications, it is desirable to maximise the weight in the preserved subspace. This is a monotonic function in the deviation q as seen from Eq. (12).

At first glance, the definition we use for the deviation from ideality q given in Eq. (19) might seem odd. However, similar metrics have been used for states in the context of QKD to quantify deviations from IID attacks [26] or from IID sources [11]. Moreover, we can establish a loose connection with a possibly more intuitive metric — the spectral norm.

Lemma 1. Let \vec{F}_{noise} and \vec{F}_{ideal} be k -element POVMs such that $\|F_i^{\text{noise}} - F_i^{\text{ideal}}\|_{\infty} \leq \delta$ for all $i \in \{1, 2, \dots, k\}$. Then $\vec{F}_{\text{noisier}} - \frac{1}{1+k\delta}\vec{F}_{\text{ideal}} \geq 0$, where \vec{F}_{noisier} is a POVM with $F_i^{\text{noisier}} = \frac{1}{1+k\delta}F_i^{\text{noise}} + \frac{\delta}{1+k\delta}\mathbb{I}$.

Proof. The proof follows from straightforward algebra after noting that $\|F_i^{\text{noise}} - F_i^{\text{ideal}}\|_{\infty} \leq \delta$ implies that $F_i^{\text{noise}} - F_i^{\text{ideal}} \geq -\delta\mathbb{I}$. \square

Given some noisy POVM \vec{F}_{noise} with k events such that $\|F_i^{\text{noise}} - F_i^{\text{ideal}}\|_{\infty} \leq \delta$ for all $i \in \{1, 2, \dots, k\}$, we can implement the noisier POVM \vec{F}_{noisier} via a classical post-processing that with probability $\frac{\delta}{1+k\delta}$ discards the measured outcome and uniformly randomly assigns it to another outcome. This can then be used with Lemma 1 and Theorem 3 to reduce the analysis of this POVM to that of the ideal POVM \vec{F}_{ideal} .

V. APPLICATION TO QKD

We now detail the application of our results to QKD protocols. As there are multiple techniques to prove the security of a QKD protocol, we shall describe the extent to which Theorems 1 to 3 can be used in each of these frameworks.

Our method relies on the flag-state squasher, which currently is not compatible with entropic uncertainty relation (EUR)-based proofs [10, 27], and phase-error correction based proofs [28]. Thus, Theorems 1 to 3 cannot be applied for such security proofs. While there already exists a finite-size security proof for basis-efficiency mismatch in the EUR framework [10], an alternate [29] proof could be obtained by incorporating the flag-state squasher into these proof techniques and then using Theorems 1 and 2.

Security proofs based on entropy accumulation theorem (EAT) [30, 31] can be directly used with the flag-state squasher [32, Appendix B]. Thus, Theorems 1 to 3 can be directly applied to accommodate imperfect detection setups in these proofs via [32, Theorem 5].

In the rest of this section we explain how to apply our results to the postselection technique [20, 26]. In particular, the postselection technique is not directly compatible with the flag-state squasher due to the ad hoc constraint described in Eq. (12). However, as we shall elaborate on, we can indirectly use Theorem 1 with the weight-preserving flag-state squasher (WPFSS) [20, Lemma 7] to prove security using the postselection technique.

A. Application to the postselection technique

We will first explain the problem of applying Theorems 1 to 3 to the postselection technique at an intuitive level before formally stating the problem and solution.

The postselection technique is a security proof technique that follows a route that reduces a security proof against the most general attack to a security proof against a limited iid attack. This reduction incurs a dimensional-dependent penalty to both the security parameter, as well as the key length. In order to facilitate its application to optical protocols, a squashing map must be used [20, Lemma 6] to reduce the dimension of the problem, and hence reduce the penalty. However, the flag-state squasher uses the subspace estimation (Eq. (12)) from the infinite-dimensional state [33]. Thus, as explained in [20, Section IV.B.1], in order to use the flag-state squasher with the postselection technique, one can follow the route first to use the weight-preserving flag-state squasher (WPFSS) [34] to facilitate the use of the postselection technique, and then the flag-state squasher can be used on the resulting POVM. Note the two distinct uses of squashing maps — first, the WPFSS *before* using the postselection technique, and then the flag-state squasher (acts on the POVM already squashed by the WPFSS) *after* using the postselection technique.

Now, it might be expected that Theorems 1 and 2 can be used after the flag-state squasher (which was used on the POVM squashed by the WPFSS) to prove security against untrusted loss and dark counts. However, the WPFSS requires that all the ‘fine-grained’ click patterns that constitute the ‘coarse-grained’ event e used to find the bound in Eq. (12) be written as a single POVM element before it can be used. As a result, the flag-state squasher is not applied on the full ‘fine-grained’ POVM consisting of all click patterns, it is instead applied on a ‘coarse-grained’ POVM that bundles together some set of click-patterns into a single element. Thus, we need to carefully check that the dark count post-processing on the coarse-grained POVM satisfies Eqs. (13) to (15) before using Theorem 1 to this situation.

We will first formally explain what it means to ‘coarse-grain’ the POVM so that we can formally state the proof idea. A ‘coarse-graining’ is a classical post-processing step whose corresponding stochastic matrix only consists of 1s and 0s. For example, consider the passive BB84 detection setup and classically post-process all click patterns that consist of more than a single click into a single ‘multi-click’ event. The stochastic matrix corresponding to this post-processing is given by

$$\mathcal{P}_{\text{cg}} = \begin{pmatrix} 1 & 0 & 0 & 0 & \overbrace{0 \dots 0}^{12} \\ 0 & 1 & 0 & 0 & 0 \dots 0 \\ 0 & 0 & 1 & 0 & 0 \dots 0 \\ 0 & 0 & 0 & 1 & 0 \dots 0 \\ 0 & 0 & 0 & 0 & 1 \dots 1 \end{pmatrix}. \quad (23)$$

The general framework is shown in Fig. 4. It is similar to the framework described in Section III. Once again, each equivalence is an equivalence of quantum-to-classical measurement channels.

- We start by considering a generic detection setup that uses threshold detectors with dark counts. Additionally, we allow for some classical post-processing \mathcal{P}'_{cg} . Although, this can be chosen to be any arbitrary post-processing, we choose it to be a coarse-graining for simplicity.

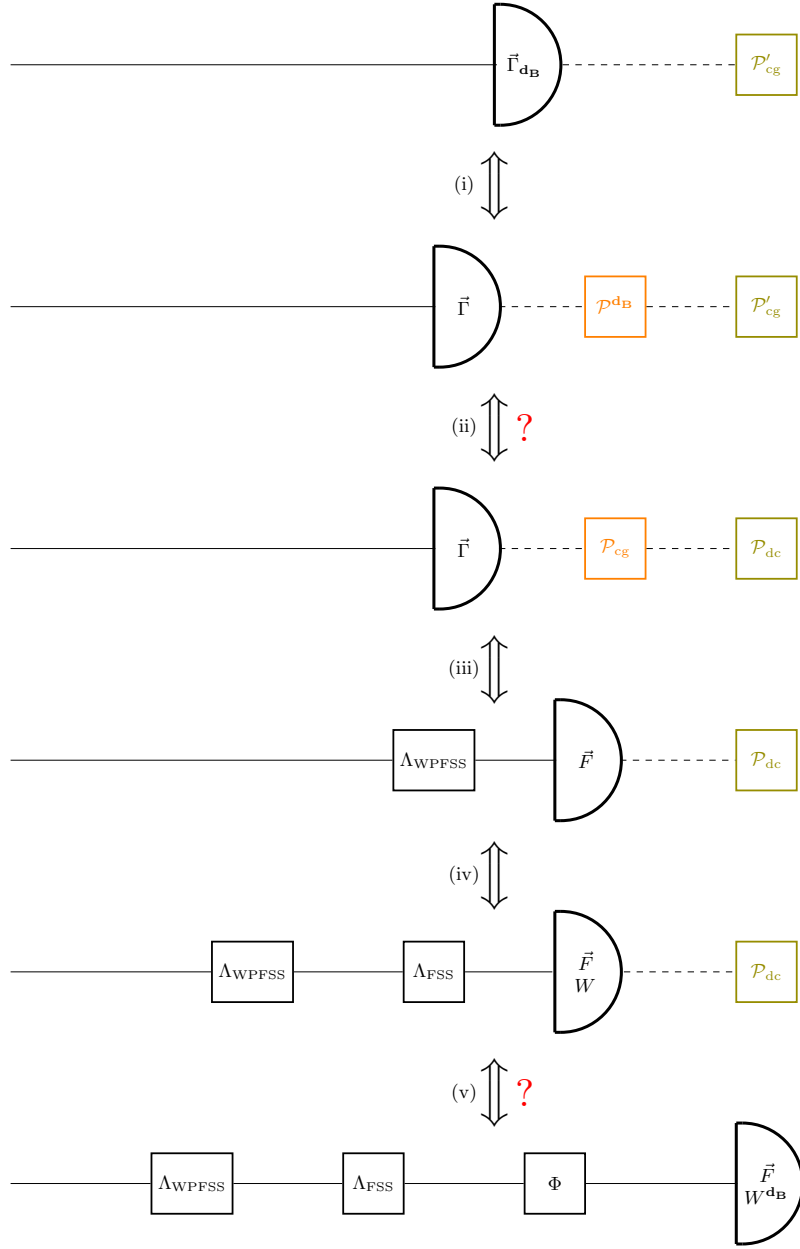


FIG. 4. A set of equivalences (as quantum-to-classical measurement channels) of detection setups to use Theorem 1 with the postselection technique. Here, \mathcal{P}'_{cg} represents the classical post-processing carried out in the protocol, \mathcal{P}^{dB} is the dark count post-processing, \mathcal{P}_{cg} is the coarse-graining required for the WPFSS Λ_{WPFSS} , and \mathcal{P}_{dc} is the post-processing fixed by Eq. (24). In the figure, olive post-processing maps represent free choices that can be made to make equivalences (ii) and (v) hold. Orange post-processing maps represent stochastic processes fixed by equivalences (i) and (iii).

- Equivalence (i) follows from the fact that dark counts can be modelled as a classical post-processing \mathcal{P}^{dB} as described in Section II A.
- Equivalence (ii) must be shown to hold, similar to the discussion in Section III 1; we need to find some stochastic matrix \mathcal{P}_{dc} such that

$$\mathcal{P}'_{cg}\mathcal{P}^{dB} = \mathcal{P}_{dc}\mathcal{P}_{cg}. \quad (24)$$

Here \mathcal{P}_{cg} is the coarse-graining required for the WPFSS.

- Equivalence (iii) follows from the existence of the WPFSS [20, Lemma 7]. The postselection technique can then be used on the resulting finite-dimensional systems.

- Equivalence (iv) follows from the existence of the flag-state squasher [21, Theorem 1].
- Equivalence (v) follows from Theorem 1, if \mathcal{P}_{dc} satisfies Eqs. (13) to (15).

The validity of equivalences (ii) and (v) depends on the coarse-graining \mathcal{P}_{cg} needed for the WPFSS. As explained above, the coarse-graining \mathcal{P}_{cg} must have the event used to bound the weight outside the preserved subspace (Eq. (12)) as one of the POVM elements. In general, for different protocol dependent choices [12, 24] of the weight estimation event, these equivalences would have to be checked on a case-by-case basis. Fortunately, for the more generic choice of weight estimation event described in Ref. [25, Section VII. F.], we can check the validity of these equivalences *independent* of protocol choice, which we now proceed to discuss.

The weight estimation in [25], which can be applied to any passive detection setup, uses the event consisting of any click pattern with more than a single-click. The coarse-graining \mathcal{P}_{cg} corresponding to this weight estimation event does nothing to the no-click and single-click event, but considers the rest of the events to be a single multi-click event. Concretely, the stochastic matrix corresponding to this coarse-graining is given by

$$\mathcal{P}_{\text{cg}} = \begin{pmatrix} 1 & 0 \dots 0 & 0 \dots 0 \\ 0 & \mathbb{I}_{n_S} & \mathbf{0}_{n_S \times n_M} \\ \vdots & & \\ 0 & & \\ 0 & \underbrace{0 \dots 0}_{n_S} & \underbrace{1 \dots 1}_{n_M} \end{pmatrix}, \quad (25)$$

where n_S is the number of single-click events, and n_M is the number of multi-click events.

For this coarse-graining, we shall verify that there exists a classical post-processing \mathcal{P}_{dc} that satisfies Eq. (24). First, we set the coarse-graining \mathcal{P}'_{cg} performed in the protocol to be the same as the coarse-graining \mathcal{P}_{cg} described in Eq. (25). Further, we need to make the physically motivated assumption that the dark count post-processing \mathcal{P}^{dB} does not turn multi-clicks into no-click or single-click events, i.e.

$$\mathcal{P}_{i|m}^{\text{dB}} = 0, \quad (26)$$

for all $i \in \{0\} \cup S$, and $m \in M$. Thus, the dark count post-processing can be written as a block-matrix whose top-right block is zero as

$$\mathcal{P}^{\text{dB}} = \begin{pmatrix} \overbrace{\mathcal{P}_{M^C|M^C}^{\text{dB}}}^{n_S+1} & \overbrace{\mathbf{0}_{(n_S+1) \times n_M}}^{n_M} \\ \mathcal{P}_{M|M^C}^{\text{dB}} & \mathcal{P}_{M|M}^{\text{dB}} \end{pmatrix}. \quad (27)$$

Importantly, the $\mathbf{0}_{(n_S+1) \times n_M}$ block along with the fact that $\mathcal{P}_{M|M}^{\text{dB}}$ is a stochastic matrix can be used to verify from explicit computation that the following ansatz satisfies Eq. (24):

$$\mathcal{P}_{\text{dc}} = \begin{pmatrix} \overbrace{\mathcal{P}_{M^C|M^C}^{\text{dB}}}^{n_S+1} & \begin{matrix} 0 \\ \vdots \\ 0 \end{matrix} \\ \hline s_{M|M^C}^1 \dots s_{M|M^C}^{n_S+1} & 1 \end{pmatrix}, \quad (28)$$

where $s_{M|M^C}^i$ is the sum of all elements in the i^{th} column of $\mathcal{P}_{M|M^C}^{\text{dB}}$.

Moreover, it is straightforward to verify that this post-processing \mathcal{P}_{dc} satisfies Eqs. (13) to (15). Thus, Theorem 1 can be used to show that equivalence (v) holds. We have hence shown that the postselection technique can be used with the results of this paper with an appropriate choice of coarse-graining \mathcal{P}_{cg} .

Technical aside 1 (Application to dimension reduction method). The dimension reduction method [35] is a generic tool that bounds the optimal value of an SDP A with a smaller SDP A_{proj} constructed by projecting the optimisation variables used in SDP A into a smaller subspace. Thus, it is a useful tool to reduce the computational resources used for numerical key rate computations.

As it is a simplification at the level of the single-round key rate semidefinite program (SDP), it can be directly used with the results of this paper as an additional component after constructing the noise channel with the help of the flag-state squasher. This simplifies the numerical computations significantly [35, Fig. 9].

VI. CONCLUSION

In this work, we develop a general framework for rigorously addressing imperfections in detection setups. We accomplish this by constructing a channel that ‘gives’ the imperfection to the adversary Eve. The portion ‘given’ to Eve is formalised through a classical ‘tagged’ space as in the flag-state squasher [21]. We have phrased our results generically to facilitate their application to a variety of adversarial tasks beyond the immediate use in QKD security proofs. While our theoretical results can be stated generically (see Theorem 3), the usage of this theorem requires some notion of an ideal POVM \vec{F}_{ideal} , and the estimation of the deviation from ideality q as detailed in Section IV B 3. Since deriving this data directly from experimentally measurable quantities is challenging, we use physically motivated models for threshold detectors that include dark counts and non-unit efficiencies.

Specifically, we assume that for all detectors used in the detection setup the dark count rates and efficiencies have specific values (possibly chosen by Eve) within some given range. We emphasise that such a range is typically obtained in characterisation experiments (for e.g. as directed in [36, Table 4.3]). Thus, our specialised theorems for dark counts (Theorem 1) and loss (Theorem 2) addresses this practically relevant situation. The amount ‘given’ to Eve in this case depends on the maximum dark count rate and the difference in the maximum and minimum efficiency of all the detectors used in the detection setup.

We have also detailed the application of our work to a variety of QKD security proof techniques. Specifically, our results can be directly applied to EAT-based techniques via [32, Theorem 5], and we describe the steps required to apply our results to the postselection technique. More work is needed to apply our techniques to EUR and phase-error based frameworks. One way to accomplish this task is by making the flag-state squasher compatible with these proof techniques. Indeed, this would constitute an alternate (to [10]) security proof in the presence of basis-dependent loss.

An interesting extension of our work would be to use our framework and construct noise channels (correlated over protocol rounds) for afterpulsing and detector dead times. Additionally, more work must be done to characterise the deviation from ideality q for arbitrary detection setups, for example, to incorporate imperfectly characterised beam-splitters.

ACKNOWLEDGMENTS

We thank Joe Itoi for discussions regarding Section III A. The work has been performed at the Institute for Quantum Computing, at the University of Waterloo, which is supported by Innovation, Science, and Economic Development Canada. The research has been supported by NSERC under the Discovery Grants Program, Grant No. 341495.

Appendix A: Numerically checking the existence of a noise channel

In this appendix we describe a numeric method to check Eqs. (4) and (5) for generic protocols with any squashing map, but for a specific value of the dark count rates $\mathbf{d}_{\mathbf{B}}$ and loss η . Since it requires a specific value of the dark count rates $\mathbf{d}_{\mathbf{B}}$ and loss η (and although the analysis can be repeated a finite number of times for different values of $\mathbf{d}_{\mathbf{B}}$, η), this method does not constitute a rigorous treatment of untrusted dark counts. However, it serves as a useful tool when searching for a possible post-processing that satisfies equation Eq. (4), and a possible noise channel satisfying Eq. (5).

1. Eq. (4) as a linear program

$$\mathcal{P}'_{\text{sq}} \mathcal{P}^{\mathbf{d}_{\mathbf{B}}} = \mathcal{P}_{\text{dc}} \mathcal{P}_{\text{sq}}$$

Under the simplifying assumption that $\mathcal{P}'_{\text{sq}} = \mathcal{P}_{\text{sq}}$, it is clear that this is just a linear constraint for the variable \mathcal{P}_{dc} . In addition to this constraint, we need to constrain it to be a stochastic matrix, i.e., all entries need to be positive and each row needs to sum to 1. As these are all linear constraints, this is a linear program (where we only need to find a feasible point).

2. Eq. (5) as a semidefinite program

$$\mathcal{P}_{\text{dc}} \text{Tr}[\vec{F}_\eta \rho] = \text{Tr}[\vec{F} \Phi_{\text{dB}, \eta}(\rho)] \quad \forall \rho$$

Here \mathcal{P}_{dc} is obtained from Appendix A1. This can be rephrased using the Choi isomorphism J of the noise channel Φ as

$$\mathcal{P}_{\text{dc}} \text{Tr}[\vec{F}_\eta \rho] = \text{Tr}\left[\left(\rho^\top \otimes \vec{F}\right) J\right] \quad \forall \rho. \quad (\text{A1})$$

It is sufficient to satisfy Eq. (A1) on a (finite) set of ρ that constitutes a basis for the space. This gives a finite set of linear constraints on the Choi map J . Additionally, since J is the Choi representation of a channel, it must be positive semidefinite, and tracing over the second space must give the identity on the first space. All of these are positive semidefinite or linear constraints and thus this constitutes a semidefinite program (where we only need to show there exists a feasible point).

As we are not using this as a rigorous proof technique — we only use it as an intuition building tool — we do not worry about numerical imprecision.

Appendix B: Noise channel constructions

Theorem 1 (Dark count noise channel). Let $\vec{\Gamma}_{\text{dB}, \eta}$ be the POVM for a threshold detection setup with independent dark counts, where each $\Gamma_i^{\text{dB}, \eta} = \Gamma_{i,0}^{\text{dB}, \eta} \oplus \Gamma_{i,m=1}^{\text{dB}, \eta} \oplus \Gamma_{i,m>1}^{\text{dB}, \eta}$ is block-diagonal with an associated Hilbert space $\mathcal{H}_0 \oplus \mathcal{H}_1 \oplus \mathcal{H}_{m>1}$ corresponding to the total photon number. Then there exists a flag-state squashing map $\Lambda : \mathcal{H}_0 \oplus \mathcal{H}_1 \oplus \mathcal{H}_{m>1} \rightarrow \mathcal{H}_{m \leq 1} \oplus \mathcal{H}_F$, and a noise channel $\Phi_{\text{dB}} : \mathcal{H}_0 \oplus \mathcal{H}_1 \oplus \mathcal{H}_F \rightarrow \mathcal{H}_0 \oplus \mathcal{H}_1 \oplus \mathcal{H}_F$ such that $\text{Tr}[\vec{\Gamma}_{\text{dB}, \eta} \rho] = \text{Tr}[\vec{F}_\eta \Phi_{\text{dB}}(\Lambda(\rho))]$ for all density matrices ρ . Here,

$$F_i^\eta = \Gamma_{i,m=0}^\eta \oplus \Gamma_{i,m=1}^\eta \oplus |i\rangle\langle i|,$$

where $|i\rangle$ forms an orthonormal basis for the flag space \mathcal{H}_F . Moreover for any density matrix ρ ,

$$\text{Tr}[\Phi_{\text{dB}}(\rho) \Pi_{\leq 1}] = \mathcal{P}_{0|0}^{\text{dB}} \text{Tr}[\rho \Pi_{\leq 1}], \quad (17)$$

where $\Pi_{\leq 1}$ is the projection onto the space $\mathcal{H}_0 \oplus \mathcal{H}_1$, and \mathcal{P}^{dB} is the stochastic matrix that models the dark counts.

Proof. The existence of the flag-state squasher is directly proved in [21, Theorem 1]. Note that since \mathcal{H}_0 is one-dimensional, this can also serve as the flag for the no-click event. We make an ansatz for the noise channel, depicted in Fig. 5 which we will now elaborate on. The noise channel first projects the input state into \mathcal{H}_1 and $\mathcal{H}_0 \oplus \mathcal{H}_F$. On $\mathcal{H}_0 \oplus \mathcal{H}_F$, it first measures the state with the lossy POVM \vec{F}_η , and then applies the dark count post-processing map on the measurement results.

On \mathcal{H}_1 , it probabilistically chooses between two channels. With probability $\mathcal{P}_{0|0}^{\text{dB}}$, it acts as the identity channel. Intuitively, this corresponds to the case when there are no dark counts in the setup. When there are dark counts, we assign the detection events to classical states in the flag-space as follows. With probability $1 - \mathcal{P}_{0|0}^{\text{dB}}$, the noise channel measures the state with \vec{F}_η to obtain result $\vec{p} = \text{Tr}[\vec{F}_\eta \rho_1]$, where ρ_1 is the part of ρ acting on \mathcal{H}_1 . The noise channel then uses the measurement result \vec{p} to prepare the classical state

$$\tau_{\text{C}} = \frac{1}{1 - \mathcal{P}_{0|0}^{\text{dB}}} \left(\sum_{\substack{m \in M \\ j \notin M}} \mathcal{P}_{m|j}^{\text{dB}} p_j |m\rangle\langle m| + \sum_{s \in S} \left(\mathcal{P}_{s|0}^{\text{dB}} p_0 + (\mathcal{P}_{s|s}^{\text{dB}} - \mathcal{P}_{0|0}^{\text{dB}}) p_s \right) |s\rangle\langle s| \right). \quad (\text{B1})$$

The rest of the proof follows by proving the following:

1. Φ is completely-positive and trace-preserving (CPTP),
2. $\mathcal{P}^{\text{dB}} \text{Tr}[\vec{F}_\eta \rho] = \text{Tr}[\vec{F}_\eta \Phi(\rho)]$ for all input density matrices ρ ,

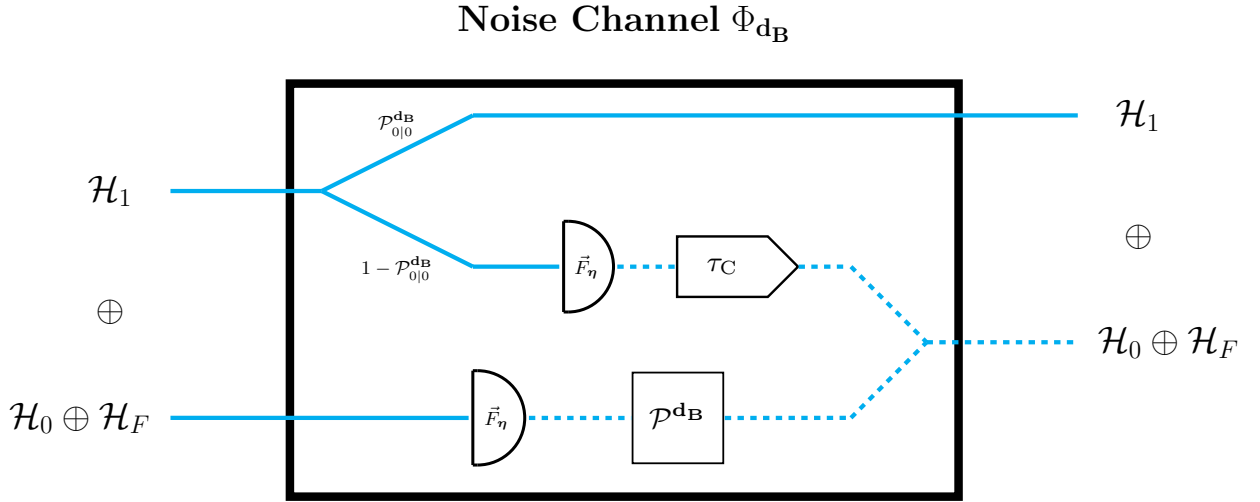


FIG. 5. Constructive description of the noise channel. Each line corresponds to a subspace of the input Hilbert space associated with the block-diagonal decomposition of the POVM elements. The dashed lines refer to classical states.

$$3. \text{Tr}[\Phi(\rho)\Pi_{\leq 1}] \leq \mathcal{P}_{0|0}^{\text{dB}} \text{Tr}[\rho\Pi_{\leq 1}] \text{ for all } \rho.$$

Φ is CPTP: Since it is clear that measurements and classical post-processing are physical channels, Φ can be shown to be CPTP by showing that τ_C is a valid classical state as the CPTP property is preserved under channel composition. Note that all the elements of τ_C are positive as all elements of the stochastic matrix \mathcal{P}^{dB} are positive, and $\mathcal{P}_{s|s}^{\text{dB}} \geq \mathcal{P}_{0|0}^{\text{dB}}$ for all $s \in S$ as described in Eq. (15). Also, note that $\sum_{j \notin M} p_j = 1$ as $p_m = 0$ for all $m \in M$ as stated in Eq. (16). Then we compute,

$$\begin{aligned} \text{Tr}[\tau_C] &= \frac{1}{1 - \mathcal{P}_{0|0}^{\text{dB}}} \left(\sum_{\substack{m \in M \\ j \notin M}} \mathcal{P}_{m|j}^{\text{dB}} p_j + \sum_{s \in S} \left(\mathcal{P}_{s|0}^{\text{dB}} p_0 + (\mathcal{P}_{s|s}^{\text{dB}} - \mathcal{P}_{0|0}^{\text{dB}}) p_s \right) \right) \\ &= \frac{1}{1 - \mathcal{P}_{0|0}^{\text{dB}}} \left(\sum_{\substack{s \in S \\ m \in M}} \left(\mathcal{P}_{m|0}^{\text{dB}} + \mathcal{P}_{s|0}^{\text{dB}} \right) p_0 + \sum_{\substack{s \in S \\ m \in M}} \left(\mathcal{P}_{m|s}^{\text{dB}} + \mathcal{P}_{s|s}^{\text{dB}} - \mathcal{P}_{0|0}^{\text{dB}} \right) p_s \right) \\ &= \frac{1}{1 - \mathcal{P}_{0|0}^{\text{dB}}} \left((1 - \mathcal{P}_{0|0}^{\text{dB}}) p_0 + \sum_{s \in S} (1 - \mathcal{P}_{0|0}^{\text{dB}}) p_s \right) \\ &= 1, \end{aligned} \tag{B2}$$

where Eq. (B2) follows from the fact that $\sum_{m \in M} \mathcal{P}_{m|s}^{\text{dB}} + \mathcal{P}_{s|s}^{\text{dB}} = 1$ for any $s \in S$ as implied by Eqs. (13) and (14).

$\mathcal{P}^{\text{dB}} \text{Tr}[\vec{F}_\eta \rho] = \text{Tr}[\vec{F}_\eta \Phi(\rho)]$ **for all input density matrices ρ :** Due to the block-diagonal structure of the POVM elements, it suffices to show that this condition holds for flag-states $\{|i\rangle\langle i|\}_{i=1}^{n_{\text{meas}}}$, vacuum state $|\text{vac}\rangle\langle \text{vac}|$ and single-photon states ρ_1 separately. Any input state can then be written as a convex combination of these states, and linearity would extend this for all states.

For any flag-state $|i\rangle\langle i|$, the condition $\mathcal{P}^{\text{dB}} \text{Tr}[\vec{F}_\eta |i\rangle\langle i|] = \text{Tr}[\vec{F}_\eta \Phi(|i\rangle\langle i|)]$ follows directly from the construction depicted in Fig. 2. This similarly holds true for the vacuum state. We now turn our attention to the single-photon states ρ_1 . We divide the computation for the single-photon states into three parts. First, consider the statistics of all

$m \in M$. Using Eq. (16), we have that

$$\begin{aligned} \text{Tr}[F_m^\eta \Phi(\rho_1)] &= \mathcal{P}_{0|0}^{\text{dB}} \text{Tr}[F_m^\eta \rho_1] + (1 - \mathcal{P}_{0|0}^{\text{dB}}) \text{Tr}[F_m^\eta \tau_C] \\ &= 0 + \sum_{j \notin M} \mathcal{P}_{m|j}^{\text{dB}} \text{Tr}[F_j^\eta \rho_1] \end{aligned} \quad (\text{B3})$$

$$= \sum_{j \in U} \mathcal{P}_{m|j} \text{Tr}[F_j^\eta \rho_1], \quad (\text{B4})$$

where Eqs. (B3) and (B4) follow from Eq. (16).

Next, we consider the statistics of all $s \in S$.

$$\begin{aligned} \text{Tr}[F_s^\eta \Phi(\rho_1)] &= \mathcal{P}_{0|0}^{\text{dB}} \text{Tr}[F_s^\eta \rho_1] + (1 - \mathcal{P}_{0|0}^{\text{dB}}) \text{Tr}[F_s^\eta \tau_C] \\ &= \mathcal{P}_{0|0}^{\text{dB}} \text{Tr}[F_s^\eta \rho_1] + \left(\mathcal{P}_{s|0}^{\text{dB}} \text{Tr}[F_0^\eta \rho_1] + (\mathcal{P}_{s|s}^{\text{dB}} - \mathcal{P}_{0|0}^{\text{dB}}) \text{Tr}[F_s^\eta \rho_1] \right) \\ &= \mathcal{P}_{s|0}^{\text{dB}} \text{Tr}[F_0^\eta \rho_1] + \mathcal{P}_{s|s}^{\text{dB}} \text{Tr}[F_s^\eta \rho_1] \\ &= \sum_{j \in U} \mathcal{P}_{s|j}^{\text{dB}} \text{Tr}[F_j^\eta \rho_1], \end{aligned} \quad (\text{B5})$$

where Eq. (B5) follows from Eqs. (13) and (16).

Finally, we consider the no-click statistics,

$$\begin{aligned} \text{Tr}[F_0^\eta \Phi(\rho_1)] &= \mathcal{P}_{0|0}^{\text{dB}} \text{Tr}[F_0^\eta \rho_1] + (1 - \mathcal{P}_{0|0}^{\text{dB}}) \text{Tr}[F_0^\eta \tau_C] \\ &= \mathcal{P}_{0|0}^{\text{dB}} \text{Tr}[F_0^\eta \rho_1] + 0 \end{aligned} \quad (\text{B6})$$

$$= \sum_{j \in U} \mathcal{P}_{0|j}^{\text{dB}} \text{Tr}[F_j^\eta \rho_1], \quad (\text{B7})$$

where the last equality follows from Eq. (14). Thus, the noise channel Φ is a CPTP map that satisfies Eq. (5).

$\text{Tr}[\Phi(\rho)\Pi_{\leq 1}] \leq \mathcal{P}_{0|0}^{\text{dB}} \text{Tr}[\rho\Pi_{\leq 1}]$ **for all** ρ : Given some density matrix ρ , we let $\Pi_{\leq 1}\rho\Pi_{\leq 1} = q_0 |\text{vac}\rangle\langle\text{vac}| + q_1 \rho_1$. From the construction depicted in Fig. 5, we see that $\Phi(|\text{vac}\rangle\langle\text{vac}|) = \mathcal{P}_{0|0}^{\text{dB}} |\text{vac}\rangle\langle\text{vac}| + \sum_{i \neq 0} \mathcal{P}_{i|0}^{\text{dB}} |i\rangle\langle i|$. Moreover, $\Phi(\rho_1) = \mathcal{P}_{0|0}^{\text{dB}} \rho_1 + \tau_C$, where τ_C is composed entirely of flags. Finally, $\Phi(|i\rangle\langle i|)$ only has support on the flag space \mathcal{H}_F . Thus, $\Pi_{\leq 1}\Phi(\rho)\Pi_{\leq 1} = q_0 \mathcal{P}_{0|0}^{\text{dB}} |\text{vac}\rangle\langle\text{vac}| + q_1 \mathcal{P}_{0|0}^{\text{dB}} \rho_1$. Since $q_0 + q_1 = \text{Tr}[\Pi_{\leq 1}\rho]$, we have that $\text{Tr}[\Pi_{\leq 1}\Phi(\rho)] = \mathcal{P}_{0|0}^{\text{dB}} \text{Tr}[\Pi_{\leq 1}\rho]$. \square

Theorem 2 (Loss noise channel). Let $\vec{\Gamma}_\eta$ be the POVM for a threshold detection setup with loss (and without dark counts), where for each POVM outcome i , $\Gamma_i^\eta = \Gamma_{i,m \leq 1}^\eta \oplus \Gamma_{i,m > 1}^\eta$ is block-diagonal with an associated Hilbert space $\mathcal{H}_{m \leq 1} \oplus \mathcal{H}_{m > 1}$ corresponding to the total photon number. Let η_{\min} and η_{\max} be the minimum and maximum of all the detector efficiencies used in the detection setup. We can then define a family of noise channels $\Phi_\eta^{\eta^*}$ and target POVMs \vec{F}_{η^*} parametrised by some parameter η^* as follows. For any value of $\eta^* \in \left[\frac{\eta_{\min}}{1 - (\eta_{\max} - \eta_{\min})}, 1 \right]$, there exists a flag-state squashing map $\Lambda : \mathcal{H}_{m \leq 1} \oplus \mathcal{H}_{m > 1} \rightarrow \mathcal{H}_{m \leq 1} \oplus \mathcal{H}_F$, and a noise channel $\Phi_\eta^{\eta^*} : \mathcal{H}_{m \leq 1} \oplus \mathcal{H}_F \rightarrow \mathcal{H}_{m \leq 1} \oplus \mathcal{H}_F$ such that $\text{Tr}[\vec{\Gamma}_\eta \rho] = \text{Tr}[\vec{F}_{\eta^*} \Phi_\eta^{\eta^*}(\Lambda(\rho))]$ for all density matrices ρ . Here,

$$F_i^{\eta^*} = \Gamma_{i,m \leq 1}^{\eta^*} \oplus |i\rangle\langle i|,$$

where $|i\rangle$ forms an orthonormal basis for the flag space \mathcal{H}_F , and $\vec{\Gamma}_{\eta^*}$ is the POVM with (common) efficiency η^* in all detectors. Moreover for any density matrix ρ ,

$$\text{Tr}[\Phi_\eta^{\eta^*}(\rho)\Pi_{\leq 1}] = \frac{\eta_{\min}}{\eta^*} \text{Tr}[\rho\Pi_{\leq 1}], \quad (\text{18})$$

where $\Pi_{\leq 1}$ is the projection onto the space $\mathcal{H}_{m \leq 1}$.

Proof. The structure of the proof is very similar to the proof of Theorem 1. First, the existence of the flag-state squasher is directly proved in [21, Theorem 1]. Let the (lossy) POVM after the application of the flag-state squasher be given by \vec{F}_η . Note that this is related to the lossless POVM \vec{F} as

$$\vec{F}_{\eta,m \leq 1} = \mathcal{P}^\eta \vec{F}_{m \leq 1}, \quad (\text{B8})$$

where

$$\mathcal{P}^\eta = \begin{pmatrix} 1 & 1 - \eta_1 & \dots & \dots & 1 - \eta_k \\ 0 & \eta_1 & \dots & \dots & 0 \\ \vdots & \vdots & \ddots & \ddots & \vdots \\ \vdots & \vdots & \vdots & \ddots & \vdots \\ 0 & 0 & \dots & \dots & \eta_k \end{pmatrix}.$$

Additionally, the flag-space portion of both the noisy, and noiseless POVMs are identical.

We will now attempt to construct POVMs and a deviation metric that satisfies Eq. (19), enabling us to use Theorem 3 to construct the noise channel for the lossy POVM \vec{F}_η . For any value of common efficiency $\eta^* \in \left[\frac{\eta_{\min}}{1 - (\eta_{\max} - \eta_{\min})}, 1 \right]$, we break up the loss post-processing \mathcal{P}^η as

$$\mathcal{P}^\eta = \frac{\eta_{\min}}{\eta^*} \mathcal{P}^{\eta^*} + \left(1 - \frac{\eta_{\min}}{\eta^*} \right) \mathcal{Q}^{\eta, \eta^*}, \quad (\text{B9})$$

where

$$\mathcal{Q}^{\eta, \eta^*} = \begin{pmatrix} 1 & 1 - \eta^* \frac{\eta_1 - \eta_{\min}}{\eta^* - \eta_{\min}} & \dots & \dots & 1 - \eta^* \frac{\eta_k - \eta_{\min}}{\eta^* - \eta_{\min}} \\ 0 & \eta^* \frac{\eta_1 - \eta_{\min}}{\eta^* - \eta_{\min}} & \dots & \dots & 0 \\ \vdots & \vdots & \ddots & \ddots & \vdots \\ \vdots & \vdots & \vdots & \ddots & \vdots \\ 0 & 0 & \dots & \dots & \eta^* \frac{\eta_k - \eta_{\min}}{\eta^* - \eta_{\min}} \end{pmatrix},$$

Thus, from Eqs. (B8) and (B9) we get

$$\vec{F}_{\eta, m \leq 1} = \frac{\eta_{\min}}{\eta^*} \mathcal{P}^{\eta^*} \vec{F}_{m \leq 1} + \left(1 - \frac{\eta_{\min}}{\eta^*} \right) \mathcal{Q}^{\eta, \eta^*} \vec{F}_{m \leq 1}. \quad (\text{B10})$$

We can then make the identification $\vec{Q}_{\eta, m \leq 1} := \mathcal{Q}^{\eta, \eta^*} \vec{F}_{m \leq 1}$, $\vec{F}_{\text{ideal}, m \leq 1} := \mathcal{P}^{\eta^*} \vec{F}_{m \leq 1}$, and $q := 1 - \frac{\eta_{\min}}{\eta^*}$ in the preserved space, and defining all POVMs to be identical in the flag-space to directly use Theorem 2 to construct a noise channel that satisfies Eq. (18). For completeness, we depict the full channel in Fig. 6. \square

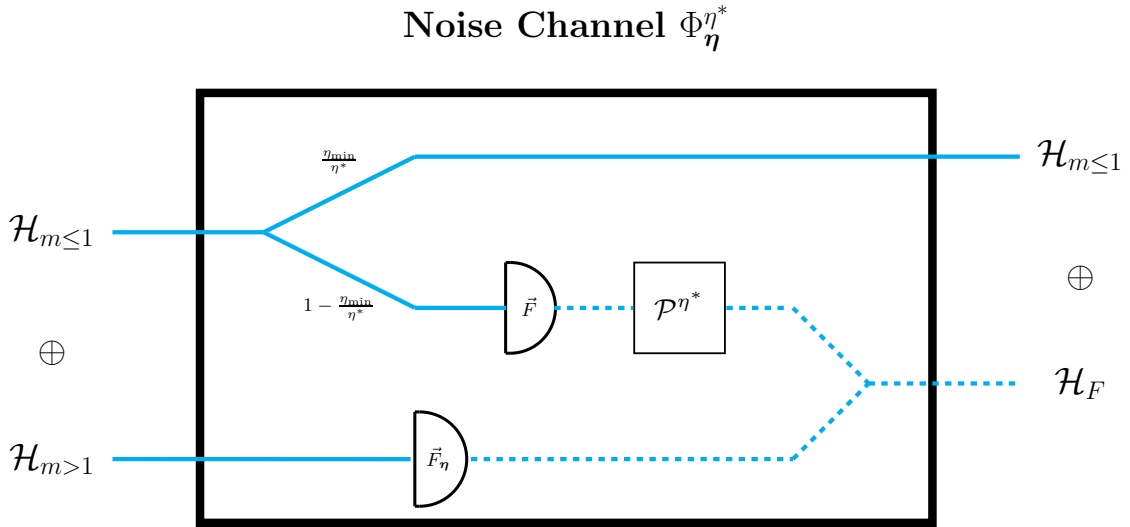


FIG. 6. Constructive description of the noise channel. Each line corresponds to a subspace of the input Hilbert space associated with the block-diagonal decomposition of the POVM elements. The dashed lines refer to classical states.

-
- [1] C. H. Bennett and G. Brassard, *International Conference on Computers, Systems & Signal Processing* **1**, pp. 175 (1984).
- [2] K. M. Audenaert and M. B. Plenio, *New Journal of Physics* **8**, 266 (2006).
- [3] K. Sulimany, S. K. Vadlamani, R. Hamerly, P. Iyengar, and D. Englund, *arXiv preprint arXiv:2408.05629* (2024).
- [4] G. Currás-Lorenzo, M. Pereira, G. Kato, M. Curty, and K. Tamaki, *arXiv preprint arXiv:2305.05930* (2023).
- [5] A. Arqand, T. Metger, and E. Y.-Z. Tan, *arXiv preprint arXiv:2407.20396* (2024).
- [6] X. Sixto, Á. Navarrete, M. Pereira, G. Currás-Lorenzo, K. Tamaki, and M. Curty, *arXiv preprint arXiv:2411.13948* (2024).
- [7] V. Zapatero, Á. Navarrete, K. Tamaki, and M. Curty, *Quantum* **5**, 602 (2021).
- [8] G. Currás-Lorenzo, S. Nahar, N. Lütkenhaus, K. Tamaki, and M. Curty, *Quantum Science and Technology* **9**, 015025 (2023).
- [9] C.-h. F. Fung, K. Tamaki, B. Qi, H.-K. Lo, and X. Ma, *arXiv preprint arXiv:0802.3788* (2008).
- [10] D. Tupkary, S. Nahar, P. Sinha, and N. Lütkenhaus, (2024), *arXiv:2408.17349* [quant-ph].
- [11] A. Marwah and F. Dupuis, *arXiv preprint arXiv:2402.12346* (2024).
- [12] N. K. H. Li and N. Lütkenhaus, *Physical Review Research* **2**, 043172 (2020).
- [13] T. H. Dao, F. Amanti, G. Andriani, F. Armani, F. Barbato, V. Bellani, V. Bonaiuto, S. Cammarata, M. Campostrini, S. Cornia, *et al.*, *Photonics* **12**, 8 (2024).
- [14] A. Migdall, S. V. Polyakov, J. Fan, and J. C. Bienfang, *Single-photon generation and detection: physics and applications* (Academic Press, 2013).
- [15] T. Tsurumaru and K. Tamaki, *Physical Review A—Atomic, Molecular, and Optical Physics* **78**, 032302 (2008).
- [16] N. J. Beaudry, T. Moroder, and N. Lütkenhaus, *Physical review letters* **101**, 093601 (2008).
- [17] T. Tsurumaru, *Physical Review A—Atomic, Molecular, and Optical Physics* **81**, 012328 (2010).
- [18] O. Gittsovich, N. J. Beaudry, V. Narasimhachar, R. R. Alvarez, T. Moroder, and N. Lütkenhaus, *Physical Review A* **89**, 012325 (2014).
- [19] T. Moroder, O. Gühne, N. Beaudry, M. Piani, and N. Lütkenhaus, *Physical Review A* **81**, 052342 (2010).
- [20] S. Nahar, D. Tupkary, Y. Zhao, N. Lütkenhaus, and E. Y.-Z. Tan, *PRX Quantum* **5**, 040315 (2024).
- [21] Y. Zhang, P. J. Coles, A. Winick, J. Lin, and N. Lütkenhaus, *Physical Review Research* **3**, 013076 (2021).
- [22] By classical we mean diagonal in the basis described by the flags.
- [23] N. K. H. Li, “Application of the Flag-State Squashing Model to Numerical Quantum Key Distribution Security Analysis,” (2020).
- [24] S. Nahar, T. Upadhyaya, and N. Lütkenhaus, *Physical Review Applied* **20**, 064031 (2023), publisher: American Physical Society.
- [25] L. Kamin and N. Lütkenhaus, *Physical Review Research* **6**, 043223 (2024).
- [26] M. Christandl, R. König, and R. Renner, *Physical review letters* **102**, 020504 (2009).
- [27] M. Tomamichel and A. Leverrier, *Quantum* **1**, 14 (2017).
- [28] M. Koashi, *New Journal of Physics* **11**, 045018 (2009).
- [29] Note that the noise channel can be adapted to be a different value in each round, thus accommodating different detection efficiencies in each round analogous to Ref. [10].
- [30] F. Dupuis, O. Fawzi, and R. Renner, *Communications in Mathematical Physics* **379**, 867 (2020).
- [31] T. Metger, O. Fawzi, D. Sutter, and R. Renner, in *2022 IEEE 63rd Annual Symposium on Foundations of Computer Science (FOCS)* (2022) pp. 844–850, ISSN: 2575-8454.
- [32] L. Kamin, A. Arqand, I. George, N. Lütkenhaus, and E. Y.-Z. Tan, *arXiv preprint arXiv:2406.10198* (2024).
- [33] Note that there exists a de Finetti theorem for infinite-dimensional states [37] that can be used with the subspace estimation, although we expect it to perform worse than the postselection theorem due to the ‘sacrifice’ bits (see figure 2 from Ref. [38] for an example comparison between the performance of the de Finetti theorem and postselection technique).
- [34] For our application here, it is not critical to understand all the details of the WPFSS. The only important detail is that the WPFSS does not allow for the usage of any fine-grained click-pattern that constitutes the event e , instead bundling them up into a single ‘coarse-grained’ POVM element.
- [35] T. Upadhyaya, T. Van Himbeeck, J. Lin, and N. Lütkenhaus, *PRX Quantum* **2**, 020325 (2021).
- [36] C. J. Chunnillall, T. Chapuran, I. P. Degiovanni, M. Gramegna, I. P. Degiovanni, M. Gramegna, S. Kück, A. Lewis, N. Lütkenhaus, A. Mink, *et al.*, “Quantum key distribution (qkd); component characterization: characterizing optical components for qkd systems,” (2016).
- [37] R. Renner and J. I. Cirac, *Physical review letters* **102**, 110504 (2009).
- [38] L. Sheridan, T. P. Le, and V. Scarani, *New Journal of Physics* **12**, 123019 (2010).